Hypersonic Viscous Drag Effects on Blunt Slender Cones

JACK D. WHITFIELD* AND B. J. GRIFFITH†
ARO, Inc., Arnold Air Force Station, Tenn.

Experimental drag data from a series of cone models are presented over a wide range of Reynolds numbers at hypersonic flow conditions. The data include Mach numbers from 9 to 22 with Reynolds numbers based on model length ranging from 600 to 500,000. Most data were obtained with test model surface temperature cold relative to the stagnation temperature; a limited amount of hot-wall data were obtained. The influence of viscous drag on the lift-drag ratio of slender blunt cones is shown experimentally and theoretically. Drag reduction by boundary-layer gas injection is shown experimentally for both cold- and hot-wall test conditions. Theoretical estimates based on existing theories are given, and the significant contributions to the zero-lift, viscous drag rise of cold-wall cones are identified as the usual "similar" or Blasius friction drag and transverse curvature effects. The theoretical estimates are shown to offer a good engineering approximation to the hypersonic viscous drag of cold-wall, blunt slender cones within the continuum flow regime.

Nomenclature

A = constant obtained by Cohen and Reshotko integral method [see Eq. (2)]
B = proportionality constant [see Eq. (3)]
C_A = total axial force at angle of attack
C_e = form of Chapman-Rubesin viscosity coefficient, $(\mu_w/\mu_e)(T_e/T_w)$
C_i = injection coefficient [see Eq. (12)]
C_∞ = form of Chapman-Rubesin viscosity coefficient, $(\mu_w/\mu_\infty)(T_\infty/T_w)$
C_* = form of Chapman-Rubesin viscosity coefficient, $(\mu_*/\mu_\infty)(T_\infty/T_*)$
C_D = total forebody drag coefficient based on base area [see Eq. (6)]
C_{D_N} = inviscid model nose drag coefficient
C_{D0} = inviscid pressure drag coefficient based on base area
$\bar{C}_{D_f}$ = total skin-friction coefficient from similar solutions based on base area
C_{D_f} = total friction drag
$(\Delta C_{D_f})_p$ = incremental increase in average skin-friction coefficient caused by induced pressure [see Eq. (3)]
$(\Delta C_D)_{tc}$ = incremental increase in average skin-friction coefficient caused by transverse curvature effects [see Eq. (5)]
$(\Delta C_D)_p$ = incremental increase in pressure drag caused by induced pressure [see Eq. (4)]
ΔC_{D_v} = viscous drag coefficient $(C_D - C_{D0})$
C_{A_α} = inviscid axial force at angle of attack
N = normal force coefficient
$\bar{C}_p$ = pressure coefficient, $(p - p_\infty)/1/2\rho_\infty u_\infty^2$
$\bar{C}_{p_c}$ = average inviscid pressure coefficient for conical section of body
$\bar{c}_f$ = local similar skin-friction coefficient, $(2\bar{\tau}_w)/(\rho_w u_e^2)$
d_B = model base diameter
d_N = model nose diameter
d_∞ = function of surface temperature, gas properties, and freestream conditions (see Ref. 19)
$F_1(K)$ = function of $M_\infty\theta_c$ (see Ref. 19)
G_B = distribution parameter (noted as B in Ref. 23)
ΔH = enthalpy potential (see Ref. 23)
h = enthalpy
L = over-all model length
L/D = lift to drag ratio
M = Mach number
$(M_e)_L$ = local surface Mach number at length L
$\dot{m}_F$ = mass rate of film flow
Pr = Prandtl number
p = pressure
$\dot{q}$ = local surface heat-transfer rate
Q = integrated heating rate
Re_w = local Reynolds number $(\rho_w \mu_e s)/\mu_w$
$Re_{\infty,L}$ = Reynolds number based on model length, $(\rho_\infty \mu_\infty L)/\mu_\infty$
r = local body radius
S_B = model base area
s = distance along model surface from stagnation point
T = temperature
T^* = reference temperature (see Ref. 7)
Tr = adiabatic wall recovery temperature
u = velocity
$\bar{v}_\infty$ = viscous parameter, $M_\infty[C_\infty/Re_{\infty,L}]^{1/2}$
$\bar{v}^*$ = viscous parameter, $M_\infty[C^*/Re_{\infty,L}]^{1/2}$
x = distance along model axis of symmetry from stagnation point
α = angle of attack
γ = ratio of specific heats
ϵ $\equiv \gamma - 1/\gamma + 1$
θ_c = cone half-vertex angle
η = angle between freestream and unit vector parallel to surface element
μ = gas viscosity
ρ = gas density
$\bar{\tau}_w$ = surface shear stress from similar solutions
χ_L = hypersonic viscous interaction parameter, $M_e^3[C_e/(\rho_e u_e L/\mu_e)]^{1/2}$
ϕ = roll angle of surface
ψ = nose bluntness ratio, r_N/r_B

Subscripts

A = test gas
B = model base dimension
e = edge of boundary-layer conditions
F = film
N = model nose dimension
0 = total stagnation conditions
w = model wall conditions
∞ = freestream conditions
1 = point of injection

Presented as Preprint 63-434 at the AIAA Conference on Physics of Entry into Planetary Atmospheres, Cambridge, Mass., August 26–28, 1963; revision received February 21, 1964. This work was sponsored by the Arnold Engineering Development Center, Air Force Systems Command, U. S. Air Force, under Contract AF 40(600)-1000 with ARO, Inc., Operating Contractor, AEDC. The authors are indebted to Clark H. Lewis for assistance with the similar solutions, J. Leith Potter for assistance in obtaining the low-density hypervelocity drag data, and H. T. Wood Jr. for assistance in obtaining the Mach 10 continuum drag data. The authors wish to express their appreciation to Bain Dayman Jr., Jet Propulsion Laboratory, California Institute of Technology, for his cooperation in permitting the use of the pneumatic launch tube to obtain the AEDC-VKF free-flight drag data and for several stimulating discussions concerning this research.

* Assistant Branch Manager, Hypervelocity Branch, von Kármán Gas Dynamics Facility. Associate Fellow Member AIAA.

† Supervisor, Aerodynamics Section, Hypervelocity Branch, von Kármán Gas Dynamics Facility. Member AIAA.

Table 1 VKF cone drag models

Model	θ_c, deg	ψ	d_B, in.	VKF tunnel	Test gas	T_w/T_0	C_{D0}
			Sting-mounted				
1	6.34	0.03	2.50	16-in. hotshot	N_2	0.1	0.030
2	6.34	0.30	2.50	16-in. hotshot	N_2	0.1	0.104
3	9	~0	0.985	16-in. hotshot	N_2	0.1	0.060
4	9	0.03	3.00	50-in. hotshot	N_2	0.1	0.063
5	9	0.03	2.50	16-in. hotshot	N_2	0.1	0.063
6	9	0.03	0.985	50-in. hotshot	N_2	0.1	0.063
7a	9	0.03	0.50	50-in. Mach 10	Air	0.75	0.063
7b	9	0.03	0.50	LDH[a]	N_2	0.2–0.25	0.063
8	9	0.30	3.00	50-in. hotshot	N_2	0.1	0.130
9	9	0.30	2.50	16-in. hotshot	N_2	0.1	0.130
10a	9	0.30	0.97	16-in. hotshot	N_2	0.1	0.130
10b	9	0.30	0.97	50-in. hotshot	N_2	0.1	0.130
11a	9	0.30	0.50	50-in. Mach 10	Air	0.75	0.130
11b	9	0.30	0.50	LDH[a]	N_2	0.2–0.25	0.130
12	13.5	0.38	4.00	16-in. hotshot	N_2	0.1	0.220
13	13.5	0.38	1.10	16-in. hotshot	N_2	0.1	0.220
14a	13.5	0.38	0.50	50-in. Mach 10	Air	0.75	0.220
14b	13.5	0.38	0.50	LDH[a]	N_2	0.2–0.25	0.220
			Free-flight				
3a	9	~0	0.50	50-in. Mach 10	Air	0.33	0.060
7c	9	0.03	0.50	50-in. Mach 10	Air	0.33	0.063
11c	9	0.30	0.50	50-in. Mach 10	Air	0.33	0.130
11d	10	~0	0.50	50-in. Mach 10	Air	0.33	0.074

[a] Low-density hypervelocity tunnel.

1. Introduction

THE often dominant role of viscous effects on the aerodynamics of slender bodies at hypersonic speeds is now widely recognized and has been the subject of many theoretical and experimental reports. The phenomena of interactions between inviscid and viscous flow fields complicate both theoretical and experimental studies of viscous effects at hypersonic speeds. The complexity of the combined problem demands recourse to both theory and experiment. Unfortunately, the available experimental data have usually been limited to supersonic rather than hypersonic speeds or to the more academic cases wherein the model surface temperature is near the total stagnation temperature. It is the purpose of this paper to present viscous drag data from slender blunt cones (Fig. 1) at hypersonic speeds with both hot and cold model surface temperatures relative to the total stagnation temperature. These experimental results were obtained from the hypersonic wind tunnels of the von Kármán Gas Dynamics Facility (VKF), Arnold Engineering Development Center (AEDC). Limited results, including tabulated zero-lift drag data, from this research have been reported by the authors.[1] Earlier preliminary data were reported[2, 3]; however, the present results (including Ref. 1) should be taken to supersede the earlier data because of improved definition of flow conditions.

During the course of this research, considerable inviscid as well as viscous dominated data were obtained from blunt slender cones. Shock shapes and pressure distributions were published by Lewis,[4] and revisions to the pressure distributions were published by Whitfield and Norfleet.[5] Inviscid hypersonic static stability data from blunt slender cones were published by Whitfield and Wolny.[6] A study of laminar heat-transfer to spherically blunted cones at hypersonic conditions was published by Griffith and Lewis.[7]

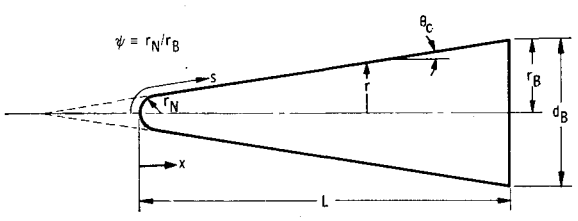

Fig. 1 Cone nomenclature.

2. Test Apparatus

The experimental data reported herein (Table 1) were obtained in four of the AEDC-VKF hypersonic wind tunnels: 1) 16-in. hypervelocity wind tunnel[3] (Hotshot 1), 2) 50-in. hypervelocity wind tunnel[3] (Hotshot 2), 3) low-density hypervelocity tunnel (LDH),[8] and 4) 50-in. Mach 10 tunnel (C).[9]

The development of the hotshot wind tunnels and their subsequent use in aerodynamic studies have been reported extensively.[1–7] It should be noted here that the definition of the flow properties is based on the method outlined by Griffith and Lewis[7] where test-section measurements of pitot pressure and stagnation heat rate are used to compute the total flow enthalpy.

The conventional sting-mounted drag models have been previously described.[1] The flow injection drag models consisted of a sharp cone forebody and a conical frustum mainbody as shown in Fig. 2. Additional information on the in-

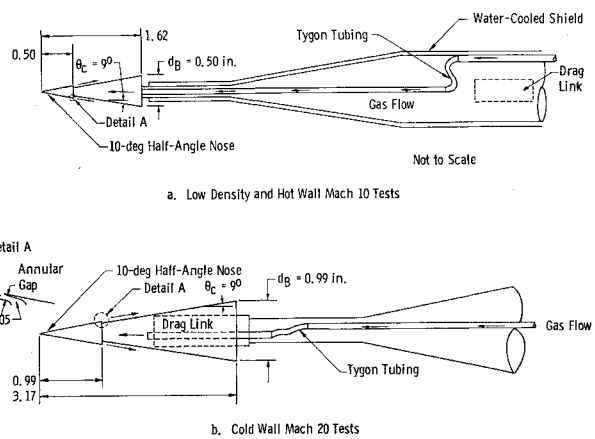

Fig. 2 Schematic of models and balances used in flow injection experiments.

Table 2 VKF flow injection models

Model	θ_c	ψ	d_B, in.	VKF tunnel	Test gas	$T_w/T_0{}^a$	C_{D_0}	Coolant
15	9	~0	0.99	50-in. hotshot	N_2	0.1	0.062	He
15	9	~0	0.99	50-in. hotshot	N_2	0.1	0.062	N_2
16	9	~0	0.50	50-in. Mach 10	Air	0.75	0.062	He
16	9	~0	0.50	LDH	N_2	0.2–0.25	0.062	He

[a] At zero injection.

jection models is tabulated in Table 2. To allow passage of the injected gas to the boundary layer, the forebody was made to overlap the front of the mainbody leaving an annular gap for the gas to be injected tangentially along the cone surface. A photograph of the model used for tests in both the low-density (LDH) and the Mach 10 (C) tunnels is shown in Fig. 3.

The free-flight drag reported herein was obtained in the 50-in. Mach 10 tunnel (C) with a pneumatic launch tube borrowed from the Jet Propulsion Laboratory (JPL). The technique and launch tube are described by Dayman.[10] Light (0.4 to 0.9 g) models were launched counter to the wind-tunnel flow at velocities of approximately 30 fps. The drag data are inferred from the distance-time data obtained by photographic means. The free-flight drag data presented here approximate a zero-lift condition. Precise angle-of-attack control was not obtained with the pneumatic launch tube, and the larger angle-of-attack runs were discarded. The data presented were obtained with $\alpha \leq 5°$ for sharp ($\psi \leq 0.03$) cones and $\alpha \leq 7°$ for the blunt cones ($\psi = 0.3$). The data have been corrected to $\alpha = 0$ by Newtonian theory[11] with the maximum corrections being 0.01 and 0.02 in C_D for the sharp and blunt cones, respectively.

3. Theoretical Considerations

Similar Solutions (No Gas Injection)

The similar solutions and integral method of Cohen and Reshotko[13, 14] were used to obtain a theoretical estimate of the Blasius-type shear stress distribution and, hence, total shear drag of the cones considered herein. The so-called "linear method' applicable when the surface temperature is constant, described in detail by Cohen and Reshotko,[14] was used with application of Mangler's transformation[15] for the axisymmetric cones considered here. The starting point of the calculation was either 1) an axisymmetric stagnation point or 2) a sharp cone point. The initial starting point 1, referred to herein as the normal shock case, assumes that all of the fluid within and immediately adjacent to the boundary layer passed through the essentially normal portion of the bow shock wave. Starting point 2, referred to as the conical shock case, assumes conditions at the outer edge of the boundary layer equal to inviscid cone surface conditions. Certainly the normal shock approximation is expected to be valid for a sufficiently blunt body at a sufficiently high Reynolds number. For the blunt cones studied here, it is suggested and later supported by the experimental data that the cones with bluntness ratios $\psi \geq 0.3$ are sufficiently blunt. Application of the conical shock case to the present study is less clear. Shock wave curvature (hence, vorticity in the cone flow field) occurs because of the "aerodynamic" bluntness induced by the boundary layer. The dominant influence of small degrees of nose bluntness at hypersonic speeds has been discussed and illustrated in the literature (e.g. Ref. 16, pp. 6–7). In general, the vorticity introduced into the flow field by the curved bow shock wave should be accounted for in the boundary-layer calculations; however, a detail analysis including vorticity is quite complex and is not considered here.

Real nitrogen thermodynamic and transport properties, as described by Grabau et al.,[12] were used in the theoretical calculations for the hypervelocity test conditions of the hot-shot tunnels. Perfect gas calculations are used for comparison with the lower temperature ($T_0 \sim 1900°$R) air tests in the 50-in. Mach 10 tunnel (C). Both the real nitrogen and perfect gas boundary-layer calculations, using Cohen and Reshotko's integral method,[14] were performed on an IBM 7070 computer.

The calculation of skin-friction coefficients (based on free-stream properties) by the integral method requires knowledge of the freestream conditions, model geometry, and pressure distribution (and hence pressure gradient distribution). The correlation of characteristics solutions and measured pressure distributions given by Lewis,[4] in terms of parameters proposed by Cheng,[17] was used to specify the pressure distributions for the blunter ($\psi \geq 0.3$) cones. Lewis' data were replotted in terms of pressure coefficient (Fig. 4) and then were assumed independent of Mach number for this application. For the sharper cones ($\psi \leq 0.03$) the normal shock case was treated by neglecting the small regime of adverse pressure gradient and using a smooth transition between a hemispherical nose pressure distribution and the inviscid, sharp cone, pressure level. Experimental cone pressure data from Whitfield and Norfleet[5] were used to specify the inviscid cone pressure, and the resulting pressure distribution for the sharper cones ($\psi \leq 0.03$) is shown in Fig. 5. The conical shock case simply assumes that the cone surface pressure is constant at the inviscid value given in Ref. 5.

The similar friction drag is, of course, a function of local flow properties; however, it is convenient for the experimentalist to base data correlations and comparisons with theory on freestream flow properties. Such an approach also serves

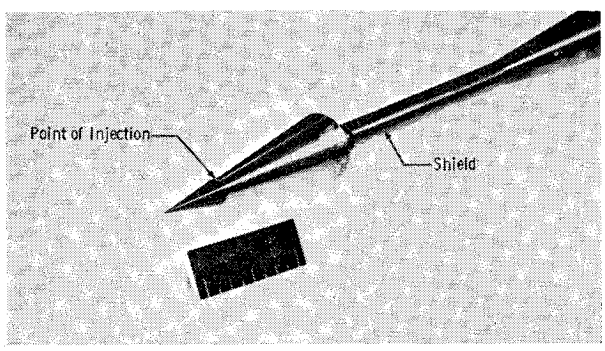

Fig. 3 Photograph of flow injection model for low density and hot-wall tests.

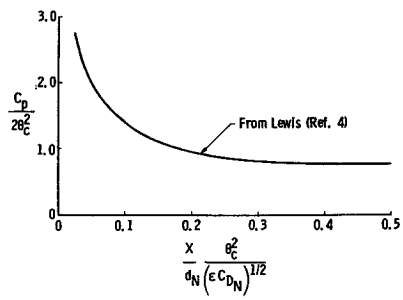

Fig. 4 Cone pressure distributions for bluntness ratios ≤ 0.3.

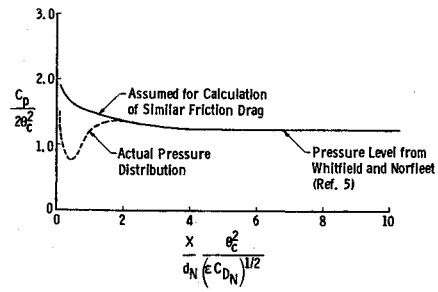

Fig. 5 Assumed and actual cone pressure distributions for bluntness ≤ 0.03.

to minimize the sometimes inconsistent (from one experimentalist to the next) estimate of local flow properties. The local similar friction drag for zero pressure gradient is, from Cohen and Reshotko,

$$\bar{c}_f(Re_w)^{1/2} = c \tag{1}$$

where $c = 0.664$ (Blasius value) in two-dimensional flow, and $c = 0.664\ (3)^{1/2} = 1.15$ in axisymmetric flow. Integrating and transforming to freestream conditions, it can be shown that the total similar drag, for both wedges and cones, is under conditions of the hypersonic strong shock approximations, represented by‡

$$\bar{C}_{Df} = A\bar{v}_\infty \tag{2}$$

where

$$\bar{v}_\infty = M_\infty[C_\infty/(Re_{\infty,L})]^{1/2}$$

The viscosity coefficient C_∞ is introduced simply to transform from local surface viscosity to freestream viscosity. The numerical solutions obtained with the pressure distributions noted herein yield the identical result, i.e., the total similar friction drag is a linear function of $\bar{v}_\infty$. The range of validity of this concept has been tested by the numerical calculations over a range of freestream Mach numbers and total temperatures (to vary the freestream and wall viscosities) with both hot- and cold-wall conditions. The results of these calculations are shown in Fig. 6. The weak Mach number dependence ($dA/dM_\infty \sim -0.005$) shown in Fig. 6 is due to the small change in the wall to freestream pressure ratio with Mach number. Within the framework of usual hypersonic approximations {i.e., $[d(p_w/p_\infty)]/dM_\infty \to 0$}, this Mach number effect tends to zero. Specific computed values of A are given in Table 3 for the various normal and conical shock cases considered.

Viscous Interaction Effects

The results from the similar solutions are based on the thin boundary-layer concept, and thus no interaction between the viscous and inviscid flow fields is considered in these solutions. Although a major portion of the experimentally observed viscous drag will be subsequently shown to be accounted for by the similar solutions, viscous drag rises consistently greater than predicted by the similar solutions are observed. The present authors[1] have, using the works of Lees and Probstein,[18] Probstein,[19] and Probstein and Elliott,[20] considered additive corrections to the similar solutions in an attempt to account for these additional viscous drag rises. These additive corrections may also, within the framework of hypersonic strong shock approximations, be shown[1] to be a

‡ The parameter $M_\infty[C_\infty/Re_{\infty,L}]^{1/2}$ arises frequently in rarefied flow analysis, hence often it is referred to as "the slip parameter"; however, the use here is in a continuum flow analysis, and hence the term "hypersonic viscous parameter" is preferred by the present authors.

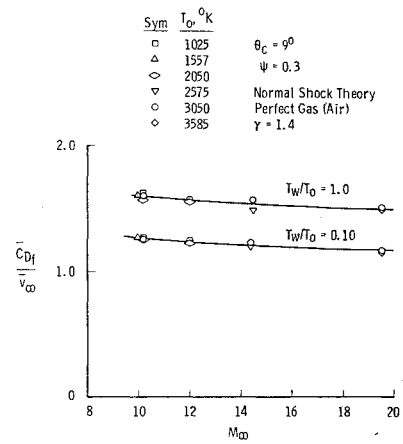

Fig. 6 Similar friction drag for various Mach numbers, wall to total temperature ratios, and freestream viscosities.

function of the hypersonic viscous parameter $\bar{v}_\infty$. The additive corrections considered are:

Displacement-Induced Pressure Drag

$$(\Delta C_D)_p \approx \tfrac{4}{3}\bar{C}_{p_c}F_1(K)d_\infty B\bar{v}_\infty \tag{3}$$

where

$$\bar{\chi}_L = B\bar{v}_\infty$$

Displacement-Induced Friction Drag

$$\frac{(\Delta C_{Df})_p}{\bar{C}_{Df}} \approx (1-\psi)\frac{3}{2}\left[\frac{-0.823}{M_e^2} + \frac{0.524}{M_e^2}\left(\frac{T_w}{T_0}\right) + 0.761\right] d_\infty F_1(K)B\bar{v}_\infty \tag{4}$$

Transverse-Curvature-Induced Friction Drag

$$\frac{(\Delta C_{Df})_{tc}}{\bar{C}_D} \approx (1-\psi)\frac{3}{2}\left[\frac{0.517}{M_e^2} + \frac{0.913}{M_e^2}\left(\frac{T_w}{T_0}\right) + 0.183\left(\frac{T_w}{T_0}\right) + 0.048\right]\frac{B\bar{v}_\infty}{(3)^{1/2}M_e\,\theta_c} \tag{5}$$

Thus, the total zero-lift drag becomes, with zero base drag,

$$C_D = C_{D_0} + (\Delta C_D)_p + \bar{C}_{Df}\left[1 + \frac{(\Delta C_{Df})_p}{\bar{C}_{Df}} + \frac{(\Delta C_{Df})_{tc}}{\bar{C}_{Df}}\right] \tag{6}$$

Examination of the various equations for each of the foregoing terms reveals that it is necessary to specify for each perfect gas case to be considered; γ, $C_p(x)$, (T_w/T_0), ψ, θ_c, and the condition of conical or normal shock wave. These specifications will permit the calculation of each drag term in the perfect gas case. Of course, when departures from a

Table 3 Results from similar solutions

θ_c, deg	ψ	Fluid	T_w/T_0	A	M_∞	B	$(M_e)_L$
Normal shock case							
6.3	0.03	N_2	0.10	1.55	19	13.9	3.01
	0.30	N_2	0.10	1.18	19	17.9	3.24
9	0.03	N_2	0.10	1.45	19	8.1	2.64
	0.03	Air	0.33	1.55	10	8.5	2.71
	0.03	Air	0.75	1.58	10	8.5	2.71
9	0.30	N_2	0.10	1.09	19	11.2	2.85
	0.30	Air	0.33	1.31	10	11.1	2.92
	0.30	Air	0.75	1.45	10	11.1	2.92
13.5	0.38	N_2	0.10	0.71	19	5.9	2.44
	0.38	Air	0.75	0.94	10	6.5	2.50
Conical shock case ($\psi = 0$)							
9	$\gamma_e = \gamma_\infty = 1.4$; $M_\infty = 10$; $(\theta_c)_{\text{eff}} \approx 9.7°$; $u_e = u_\infty$; $\bar{C}_{Df} = 1.94\bar{v}_\infty$; $\bar{\chi}_L = 35.8\bar{v}_\infty$; $M_e \sim 7.6$.						

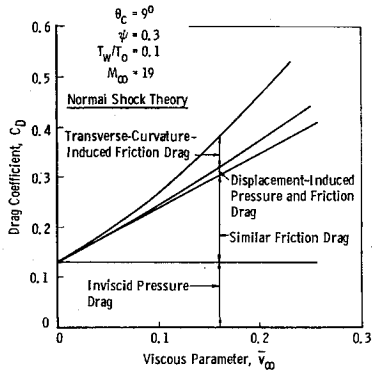

Fig. 7 Theoretical drag components for 9° half-vertex angle blunt cone.

perfect gas are to be considered, the specific flow condition must be completely defined. The perturbation terms were computed assuming constant local flow properties. Inviscid flow conditions at $x = L$ were used for these estimates.

It should be noted here that the foregoing estimate assumes a weak interaction model and thus ignores the strong interaction regime near the nose. Effects associated with flow field vorticity or with conditions where the molecular mean free path is comparable to body dimensions are not considered; thus, large values of the viscous parameter $\bar{v}_\infty$ cannot be considered. This limitation will be illustrated later by comparison with experimental data.

The primary cone model used in the experimental study is considered in detail to illustrate the relative magnitudes of the various terms of Eq. (6). This model is a blunt ($\psi = 0.3$), slender ($\theta_c = 9°$) cone considered under hypersonic ($M_\infty = 19$) cold-wall ($T_w/T_0 = 0.1$) conditions with nitrogen as a test gas. The resulting breakdown of Eq. (6) becomes, under these conditions,

$$C_D = 0.130 \text{ (inviscid pressure drag)} + 1.09\,\bar{v}_\infty \text{ (similar friction drag)} + 0.03\,\bar{v}_\infty \text{ (displacement-induced pressure drag)} + 0.47\,\bar{v}_\infty^2 \text{ (displacement-induced friction drag)} + 2.34\,\bar{v}_\infty^2 \text{ (transverse-curvature-induced friction drag)}$$

This drag estimate is illustrated in Fig. 7. For this case it is noted that the similar or Blasius-type friction drag quickly comes to dominate the zero-lift drag with decreasing Reynolds number (i.e., increasing $\bar{v}_\infty$). In general, it is found for the cold-wall case that the displacement-induced pressure drag and the displacement-induced friction drag terms are small compared to the other terms. For the hot-wall case, the displacement-induced friction drag and the transverse-curvature-induced friction drag terms become comparable.

Lift to Drag Ratio

The lift to drag ratio is assumed to consist of the following terms: 1) the total zero-lift viscous drag, 2) the inviscid pressure drag at angle of attack $C_{A\alpha}$, and 3) the normal force of the cone C_N. Therefore, the total axial force at angle of attack becomes the algebraic sum

$$C_A = (\Delta C_D)_p + \bar{C}_{D_f}\left[1 + \frac{(\Delta C_{D_f})_p}{\bar{C}_{D_f}} + \frac{(\Delta C_{D_f})_{tc}}{\bar{C}_{D_f}}\right]_{\alpha=0} + C_{A\alpha} \tag{7}$$

where $C_{A\alpha}$ is calculated from Newtonian concepts. Hence,

$$C_{A\alpha} = \frac{K_1}{\pi L^2}\int_0^L \int_0^{2\pi} x \sin^2\eta \, d\phi dx \tag{8}$$

and C_N is calculated following the correlations of Whitfield and Wolny[6] which express C_N as a function of $(2\alpha + \alpha^2/\theta_c)(1 - \psi^2)$. Finally,

$$\frac{L}{D} = \frac{C_N \cos\alpha - C_A \sin\alpha}{C_A \cos\alpha + C_N \sin\alpha} \tag{9}$$

Film Cooling by Gas Injection

An approximate method for the estimation of laminar heat-transfer and friction drag with gaseous film cooling is presented following the analysis of Swenson.[23] Consider the intermediate film model proposed by Swenson where it is assumed that the film replaces only the boundary-layer thickness of the test fluid. A heat balance of the film based on these considerations as given by Swenson is as follows:

$$(\dot{q}_A - \dot{q}_F)2\pi r\, ds = \dot{m}_F d(\Delta H_F) \tag{10}$$

Assuming $\Delta H_F = \text{const}$, $u_e = u_F$, with no mixing, $\mu = K_2 T$, where K_2 is assumed to be the same for all gases, and $p_e = p_F$, we have the results of Swenson[23]:

$$1 - \frac{Q_F}{Q_A} = \left(1 - \frac{\dot{q}_F}{\dot{q}_A}\right)_{s1/r_N} \frac{1 - e^{-G_B}}{G_B} \tag{11}$$

where G_B is given as B by Swenson.[23] The term $\dot{q}_A$ is given by Griffith and Lewis[7] for a relatively sharp cone and may be written as

$$\dot{q}_A = 0.7 M_\infty \theta_c \left(1 + \frac{2}{\gamma C_p M_\infty^2}\right)(C_*)^{1/2} \frac{[\rho_\infty u_\infty (h_0 - h_w)]}{(Re_{\infty,L})^{1/2}}$$

and defining

$$C_i = \dot{m}_F/\rho_\infty u_\infty S_B \tag{12}$$

$$\bar{v}_* = M_\infty [C_*/Re_{\infty,L}]^{1/2} \tag{13}$$

the distribution parameter G_B can be shown to be a function of $\bar{v}_*/C_i$. Assuming

$$Q_F/Q_A = (\bar{C}_{D_f})_F/(\bar{C}_{D_f})_A \tag{14}$$

we have

$$(\bar{C}_{D_f})_F/(\bar{C}_{D_f})_A = f(C_i/\bar{v}^*) \tag{15}$$

4. Experimental Results

Zero-Lift Drag without Gas Injection

Limited zero-lift drag data from the present research were previously published by Lukasiewicz et al.[2] and Whitfield and Griffith.[1] The earlier data[2] contain errors in the definition[7] of the total flow enthalpy for certain test conditions. The latter limited data[1] differ, where comparable, from the present results only by small, usually insignificant, base drag corrections. With the exception of the gas injection models, base pressure measurements were made for all of the sting-mounted AEDC-VKF models, and the total drag data were corrected to a zero base drag condition on the basis of these measurements. The measured base pressures were, for the hotshot, Mach 10, and LDH tunnels, less than p_∞, $1.2p_\infty$ and $2p_\infty$, respectively. The drag data presented from the mass injection tests represent the total measured drag, excluding the thrust component due to mass injection.

The theoretical drag estimates considered previously indicate that the total drag of a slender cone should correlate

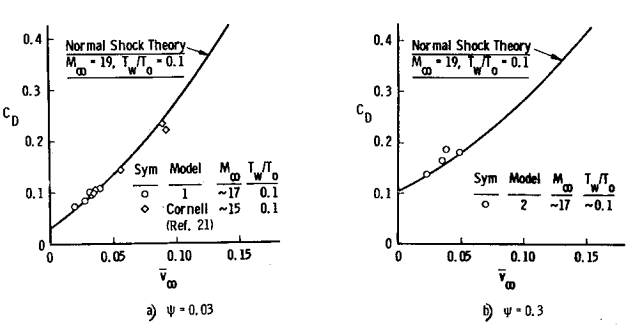

Fig. 8 Comparison of theory and experiment in continuum flow regime, 6.34° half-vertex angle cones.

with the hypersonic viscous parameter, $\bar{v}_\infty = M_\infty[C_\infty/Re_{\infty,L}]^{1/2}$. The experimental forebody drag data from 6.34°, 9°, 13.5° cones obtained within the continuum flow regime are presented as a function of the viscous parameter $\bar{v}_\infty$ in Figs. 8–10, respectively. Theoretical estimates based on the normal shock wave theoretical model are presented in all cases, and, in addition, a conical shock estimate is presented for the hot-wall, sharper 9° cone case (Fig. 9a). Experimental data from the Cornell Aeronautical Laboratory's 48-in. contoured nozzle shock tunnel[21] obtained with air as a test gas and under cold-wall, hypersonic flow conditions are also included in Figs. 8a and 9. These data are in good agreement with the hotshot data and with the theoretical estimates. Also included in Fig. 9 are hot-wall drag data obtained in the Jet Propulsion Laboratory's 21-in. hypersonic wind tunnel by Aeronutronic.[22] Reference 22 does not mention the model base pressure; however, it was assumed that the data represented total drag measurements. A base pressure of one-half freestream static pressure was assumed, and the drag data were corrected accordingly. The specific wall to stagnation temperature ratios for these data are unknown; however, it is reasonable to assume that the ratios for steady-state conditions are comparable to the present Mach 10, hot-wall ($T_w/T_0 \sim 0.75$) data.

The good agreement between the normal shock drag estimates and experiment for all of the cold-wall data in Figs. 8–10 must be considered, at present, fortuitous for the sharper 6.34° and 9° cones. Certainly, the normal shock theoretical model is violated for these sharper cone cases. An experimental check was made on the drag of a quite sharp 9° cone, and these data are included in Fig. 9a as solid symbols. Experimentally, the difference in the drag of a "sharp" ($\psi \sim 0$) cone and one with a small bluntness ($\psi = 0.03$) could not be detected. Although arguments on the influence of "aerodynamic" bluntness can be advanced, further theoretical work is required to sort out the influence of vorticity in these cases. It is interesting to note that, in spite of the mismatch between the theoretical and experimental sharper ($\psi \leq 0.03$) cone models, a good engineering approximation of the total drag within the continuum flow regime can be made by the methods presented herein. Certainly the agreement between the theoretical and experimental models is much better for the blunter ($\psi \geq 0.3$) cones, and again the theoretical model offers a good estimate of the total drags (see Figs. 8b, 9b, and 10). Griffith and Lewis[7] also found that the normal shock model gave excellent agreement between theoretical and experimental heat-transfer distributions of quite sharp cones. The hot-wall, sharp, and blunt cone drag data are also presented in Figs. 9 and 10. The experimental data are observed to be consistently above the theoretical estimates for all hot-wall models. It should be noted that the low absolute drag level required special techniques of measurement.[1]

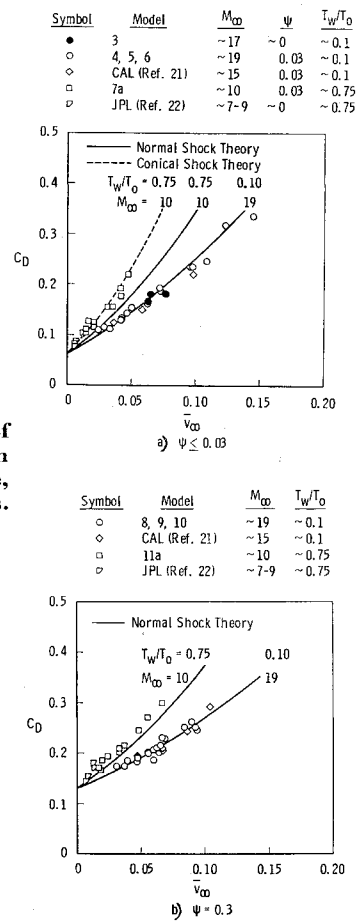

Fig. 9 Comparison of theory and experiment in continuum flow regime, 9° half-vertex angle cones.

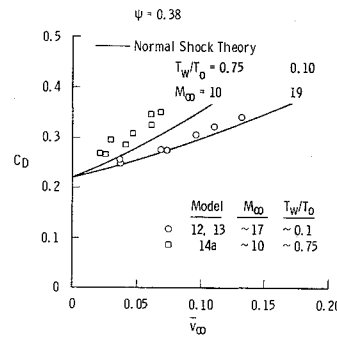

Fig. 10 Comparison of theory and experiment in continuum regime, 13.5° half-vertex angle cone.

Experimental drag data obtained under cold-wall, low-density hypersonic conditions in the LDH tunnel are compared to the higher Reynolds number data and continuum theory in Fig. 11. Continuum theoretical estimates based on the present theoretical model and corresponding to the low-density test conditions were not made because of the obviously poor match between theoretical and experimental models. It is certainly to be expected that vorticity, slip, and temperature-jump effects are present in these data in varying degrees. It is interesting to note from these drag data that the low-density ($\bar{v}_\infty > 0.3$) drag coefficients are essentially independent of the specific body shape. These data indicate that even very slender bodies will experience a drag level comparable to that of a sphere for $\bar{v}_\infty > 0.4$. Proper theoretical treatment of this important transition regime from continuum to free-molecular flow has not been accomplished and, of course, is urgently needed to better understand the flow phenomena.

During the course of the present research, Dayman[10] obtained free-flight viscous drag data from slender cones which exhibit appreciably larger viscous drag rises than the present sting-mounted data. The possibility of significant sting

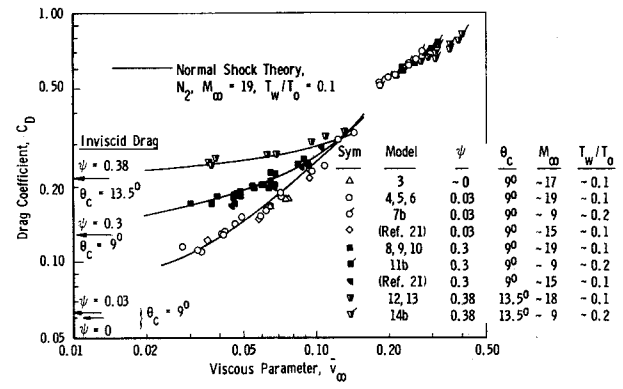

Fig. 11 Comparison of hypersonic, cold wall, viscous drag of blunt, slender cones in continuum and rarefied flow regimes.

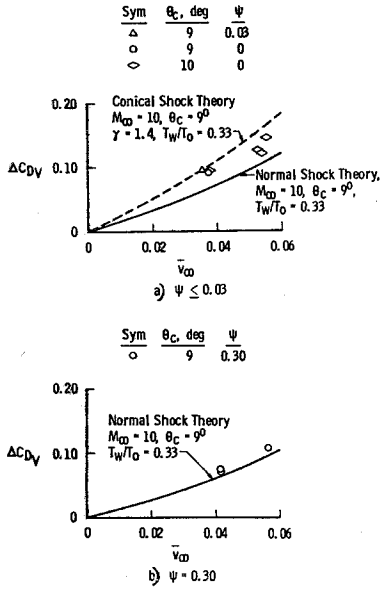

Fig. 12 Comparison of theory and free-flight drag data.

interference effects was, of course, a suspicion. The previously mentioned base pressure measurements with the identical model, sting, and wind-tunnel setups as for the drag data were made to check out this possibility. In addition, free-flight drag tests were made in the 50-in. Mach 10 (C) tunnel using Dayman's pneumatic launch tube. These free-flight data are compared to the theoretical estimates in Fig. 12. Certainly, the comparison of theory and experiment is, for these free-flight data, in keeping with the previous comparisons for the sting-mounted data. Lyons and Brady[25] also have recently published free-flight drag data for slender cones obtained in an aeroballistic range. The present data (sting-mounted and free-flight), Dayman's[10] free-flight data, Lyons and Brady's[25] free-flight data, and Wilkinson and Harrington's[21] sting-mounted data are summarized and compared to the theoretical estimates in Fig. 13. It is apparent here that reasonable agreement between theory and the experiments exists for all of the data except Dayman's. It should be noted that, in terms of base drag alone, a base pressure of approximately four times freestream static pressure would be required to explain the observed differences. This is approximately three to eight times the observed base pressures. Sting interference effects cannot, per se, explain the discrepancies, and it can only be concluded here that the present data, Lyons and Brady's[25] data, Wilkinson and Harrington's[21] data, and the theoretical considerations are self-consistent and agree reasonably well.

Lift to Drag Ratio

The simple analysis of the problem of viscous effects on the lift to drag ratio of slender blunt cones is compared with data over a limited Mach number and Reynolds number range for 9° blunt and sharp cones in Fig. 14. Note the excellent agreement between the simple theory and the experimental sharp cone ($\psi = 0.03$) data. The value of K_1 [see Eq. (8)] was taken as 2.46 following the analysis of Whitfield and Norfleet[5] on sharp slender cones at zero angle of attack.

The theory overestimates the (L/D) ratios on the blunt cone ($\psi = 0.3$). Here the constant K_1 was taken as 1.86 (accepted blunt nose value). However, referring to Cheng's[17] correlation parameter, $x\theta_c^2/d_N(\epsilon C_{D_N})^{1/2}$, one can readily see that replacing θ_c^2 by $(\theta_c + \alpha)^2$ will force the parameter to sharp cone magnitude even at moderate angles of α. Therefore, a larger value of K_1 would seem to be in order, thereby improving the comparison between theory and experiment for the blunt cone data.

Film Cooling by Gas Injection

The effect of injecting a foreign gas tangentially to the wall of a sharp 9° cone is presented in Figs. 15 and 16. The data are taken at Mach numbers 10 and 21 over a Reynolds number range of 630 to 68,300 based on model length. Both hot-wall and cold-wall data are presented and plotted vs $C_i/\bar{v}^*$ [see Eq. (15)] and compared with a theoretical computation in Fig. 16. Note that the theory predicts a more rapid reduction in the friction drag than the experimental data show. Several reasons are apparent: 1) the data include displacement-induced pressure drag, displacement-induced friction drag and transverse-curvature-induced friction drag, whereas the theory only considers the reduction in the "similar" friction drag, 2) the injection velocity and velocity outside the boundary layer are not matched, thereby causing mixing, 3) no effect on base drag and pressure drag[24] caused by the mass injection has been considered, 4) the

Symbol	Mount	M_∞	θ_c, deg	Tunnel
○	Sting	10	9	VKF-50-in. $M_\infty = 10$
◔	Sting	~19	9	VKF-50-in. Hotshot
◕	Free-Flight	10	9	VKF-50-in. $M_\infty = 10$
●	Free-Flight	10	10	VKF-50-in. $M_\infty = 10$
♦	Free-Flight	14-16	8	Ref. 25
◇	Sting	~15	9	Ref. 21
▲	Free-Flight	8	9	Ref. 10
◢	Free-Flight	8	10	Ref. 10
◀	Free-Flight	10	10	Ref. 10

Data for $0.035 \leq V_\infty \leq 0.07$

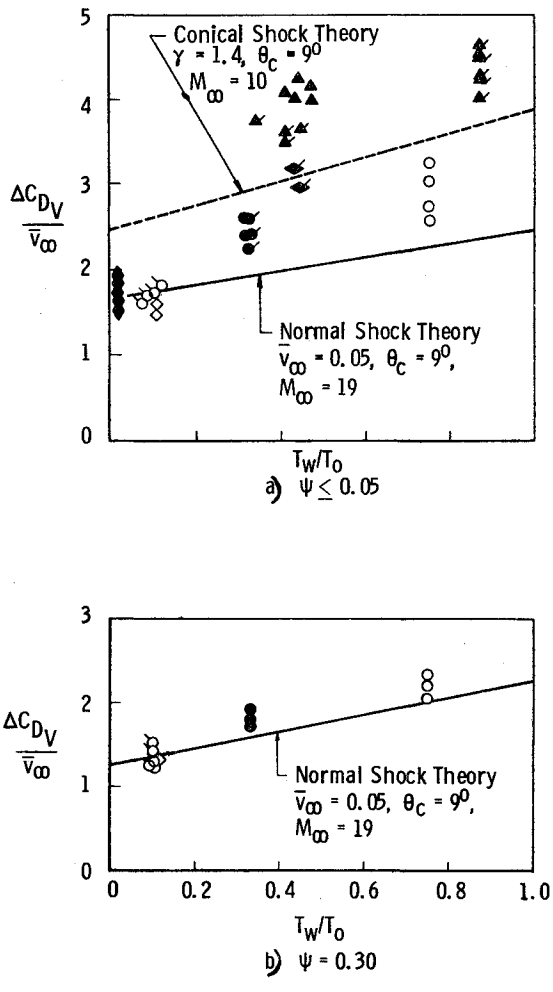

Fig. 6

Fig. 13 Comparison of sting-mounted and free-flight data with theory.

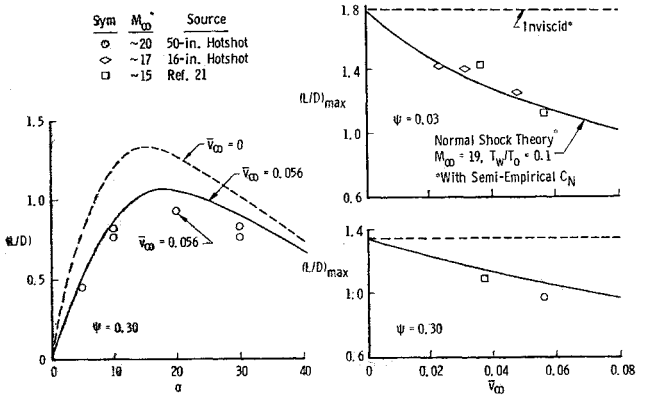

Fig. 14 Comparison of experimental and theoretical lift-to-drag ratios, 9° half-vertex angle cones, $T_w/T_0 = 0.1$.

assumption that the enthalpy potential of the injected gas (ΔH_F) is constant over the body, and 5) the assumption of the same viscosity for all gases could cause the apparent efficiency of the coolant gas to be low. The data from the low-density tunnel are not included in Fig. 16 because these data are considered to be in the transitional region between continuum and slip flow.

5. Concluding Remarks

Comparison of viscous-dominated drag data from blunt slender cones with estimates based on the theoretical work of Cohen and Reshotko and Probstein indicates good agreement for moderate values of the viscous parameter $\bar{v}_\infty$ (≤ 0.15). Agreement between theoretical estimates based on the blunt model (normal shock theory) and the experimental cold-wall data from sharp cones must be considered, at present, fortuitous. Similar agreement was not found for the hot-wall, sharper cone data. The theoretical estimates for the blunt slender cones under cold-wall, hypersonic, continuum flow conditions indicate that the dominant viscous contribution is simply the "Blasius" or similar friction drag. The primary perturbation of this similar friction drag for this cold-wall situation arises from transverse curvature effects with a relatively small influence introduced by the displacement-induced longitudinal pressure gradient. It is interesting that time-honored methods of compressible boundary-layer analysis serve to offer a reasonable engineering approximation to these quite large viscous drag rises.

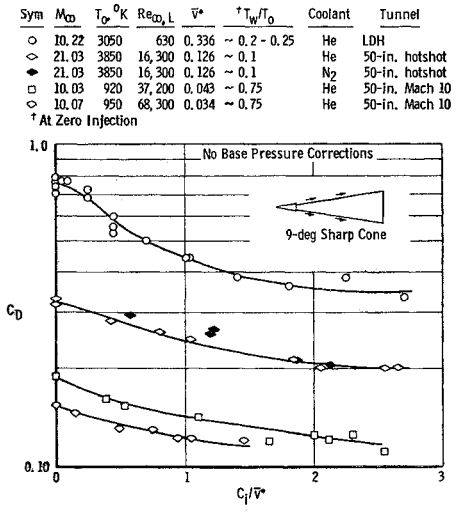

Fig. 15 Variation of zero-lift drag with mass injection, 9° half-vertex angle sharp cone.

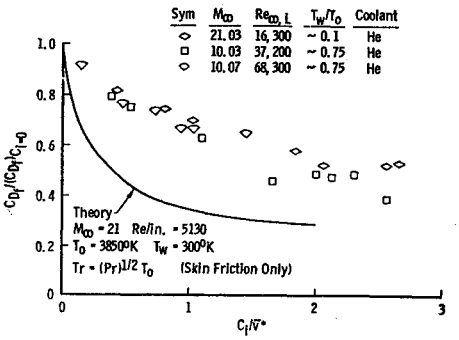

Fig. 16 Effect of mass injection on friction drag, 9° half-vertex angle sharp cone.

Within the range of blunt cone geometries studied experimentally under low-density hypersonic conditions, a significant influence of geometry was not noted. Experimental drag levels near the inviscid drag of a sphere were observed for all of the cones under these low Reynolds number, cold-wall conditions.

Discrepancies between the present viscous drag data and data from Dayman[10] at present cannot be attributed to sting interference, and the actual reason remains unexplained. It can only be concluded here that the present data, other cited free-flight data, other cited sting-mounted data, and the present theoretical considerations are self-consistent and agree reasonably well.

The agreement of the theoretical estimates of the lift to drag ratios (L/D) with the experimental data indicates that the viscous effects at zero lift and moderate angles of attack are similar.

Appreciable drag reductions result from injecting a coolant tangentially along the surface of a cone model. No significant difference was noted in using helium or nitrogen as the coolant.

References

[1] Whitfield, J. D. and Griffith, B. J., "Viscous effects on zero lift drag of slender blunt cones," Arnold Engineering Development Center, TDR-63-35 (March 1963).

[2] Lukaseiewicz, J., Whitfield, J. D., and Jackson, R., "Aerodynamic testing at Mach numbers 15 to 20," *Progress in Astronautics and Rocketry: Hypersonic Flow Research*, edited by F. R. Riddell (Academic Press, New York, 1962), Vol. 7, pp. 473–512.

[3] Lukasiewicz, J., Jackson, R., and Whitfield, J. D., "Status of development of hotshot tunnels at the AEDC," *The High Temperature Aspects of Hypersonic Flow* (Pergamon Press, London, 1964), pp. 323–356.

[4] Lewis, C. H., "Pressure distribution and shock shape over blunted slender cones at Mach numbers 16 to 19," Arnold Engineering Development Center, TN-61-81 (August 1961).

[5] Whitfield, J. D. and Norfleet, G. D., "Source flow effects in conical hypervelocity nozzles," Arnold Engineering Development Center, TDR-62-116 (June 1962).

[6] Whitfield, J. D. and Wolny, W., "Hypersonic static stability of blunt slender cones," Arnold Engineering Development Center, TDR-62-166 (August 1962); also AIAA J. 1, 486–487 (1963).

[7] Griffith, B. J. and Lewis, C. H., "A study of laminar heat-transfer to spherically blunted cones at hypersonic conditions," AIAA J. 2, 438–444 (1964).

[8] Potter, J. L., Kinslow, M., Arney, G. D., Jr., and Bailey, A. B., "Description and preliminary calibration of a low-density, hypervelocity wind tunnel," Arnold Engineering Development Center, TN-61-83 (August 1961).

[9] *Test Facilities Handbook* (Arnold Engineering Development Center, Tullahoma, Tenn., 1963), 4th ed., Vol. 4, Part 5, p. 5.5.

[10] Dayman, B., Jr., "Free-flight hypersonic viscous effects on slender cones," AIAA Preprint 64-46 (January 1964).

[11] Wells, W. R. and Armstrong, W. O., "Tables of aerodynamic

coefficients obtained from developed Newtonian expressions for complete and partial conic and spheric bodies at combined angles of attack and sideslip with some comparisons with hypersonic experimental data," NASA TR R-127 (1962).

[12] Grabau, M., Humphrey, R. L., and Little, W. J., "Determination of test-section, after-shock, and stagnation conditions in hotshot tunnels using real nitrogen at temperatures from 3000 to 4000°K," Arnold Engineering Development Center, TN-61-82 (July 1961).

[13] Cohen, C. B. and Reshotko, E., "Similar solutions for the compressible laminar boundary layers with heat transfer and pressure gradient," NACA Rept. 1293 (1956).

[14] Cohen, C. B. and Reshotko, E., "The compressible laminar boundary layer with heat transfer and arbitrary pressure gradient," NACA Rept. 1294 (1956).

[15] Mangler, W., "Compressible boundary layers on bodies of revolution," Interrogration Rept. ATI 28063, MAP-VG 83-4.7.T., English transl. (June 1946).

[16] Hayes, W. D. and Probstein, R. F., *Hypersonic Flow Theory* (Academic Press, New York, 1959), Chap. I, pp. 6–7.

[17] Cheng, H. K., "Hypersonic flow with combined leading-edge bluntness and boundary-layer displacement effect," Cornell Aeronautical Lab. Rept. AF-1285-A-4, AD 243140 (August 1960).

[18] Lees, L. and Probstein, R. F., "Hypersonic viscous flow over a flat plate," Rept. 195, Aero Engineering Lab., Princeton Univ. (April 20, 1952).

[19] Probstein, R. F., "Interacting hypersonic laminar boundary layer flow over a cone," TR AF 279811, Div. of Engineering, Brown Univ., AD 66 227 (March 1955).

[20] Probstein, R. F. and Elliott, D., "Transverse curvature effect in compressible axially symmetric laminar boundary-layer flow," J. Aeronaut. Sci. **23**, 208–224 (1956).

[21] Wilkinson, D. B. and Harrington, S. A., "Hypersonic force, pressure and heat transfer investigations of sharp and blunt slender cones," Cornell Aeronautical Lab. Rept. AF-1560-A-5 (December 1962).

[22] "Experimental investigation of the aerodynamic characteristics of 9° half-angle cones with varying degrees of nose bluntness at Mach number 9," Aeronutronic, Div. of Ford Motor Co., Publ. U-1638 (April 1962).

[23] Swenson, B. L., "An approximate analysis of film cooling on blunt bodies by gas injection near the stagnation point," NASA TN D-861 (September 1961).

[24] King, H. H., "Hypersonic flow over a slender cone with gas injection," Univ. of California, TR HE-150-205 (November 1962).

[25] Lyons, W. C., Jr. and Brady, J. J., "Hypersonic drag, stability, and wake data for cones and spheres," AIAA Preprint 64-44 (January 1964).

OCTOBER 1964 AIAA JOURNAL VOL. 2, NO. 10

Interactions of Gas Molecules with an Ideal Crystal Surface

RICHARD A. OMAN,* ALEXANDER BOGAN,† CALVIN H. WEISER,† AND CHOU H. LI‡
Grumman Aircraft Engineering Corporation, Bethpage, N. Y.

In order to increase the understanding of the interaction of gas particles with solid surfaces, we have performed some large-scale numerical computations of the classical trajectories of gas particles near a crystalline solid. Interpretations of the results of these trajectories and the corresponding responses of the lattice are given in terms of some of the dynamic similarity parameters that should control the interaction. The emphasis in this analysis is on conditions related to hypervelocity flight, where incident molecular energies are much higher than ordinary thermal energies, and collision times will approximate the natural vibrational periods of the lattice atoms. Our theoretical model, which assumes an Einstein lattice and a Lennard-Jones 6-12 potential between lattice atom and gas particle, is set up with this specific situation in mind.

Nomenclature

b = distance of closest approach to lattice atom
d = lattice-point spacing (equals edge of unit cell for simple cubic, $\frac{1}{2}$ edge for FCC and BCC)
D = depth of lattice block
D_w = dimensionless energy parameter $\epsilon/\frac{1}{2}m_g V_i^2$
E = energy
$\mathfrak{F}$ = nondimensional force
$\mathfrak{F}'$ = nondimensional force from equivalent continuum lattice
F = force
$\mathbf{i}$ = unit vector, x
$\mathbf{j}$ = unit vector, y
$\mathbf{k}$ = unit vector, z
k = spring force constant
m = mass of a particle or atom
n = number of lattice atoms in volume d^3
P = response parameter characterizing energy exchange with lattice
Q = constant used in calculation of forces
$\mathbf{r}$ = position vector of point in lattice cell (Appendix)
r = distance between incident particle and a particular lattice atom
$\mathbf{R}$ = position vector
$\mathbf{S}$ = relative position vector $\mathbf{R} - \mathbf{r}$
T = period of vibration or collision
t = time
V = velocity
W = width of lattice block
x = coordinate along surface
y = coordinate along surface
z = coordinate normal to surface
ϵ = bonding-energy parameter in Lennard-Jones 6-12 potential
ζ = coordinate in lattice (parallel to z axis)

Presented as Preprint 63-463 at the AIAA Conference on Physics of Entry into Planetary Atmospheres, Cambridge, Mass., August 26–28, 1963; revision received July 8, 1964. This work is being supported by the NASA Office of Advanced Research Programs under Contract No. NASr-104.

* Head, Gas Dynamics Group, Research Department. Member AIAA.
† Research Physicist, Research Department.
‡ Research Scientist, Research Department.